
SYNTHETIC PHOTOVOLTAIC AND WIND POWER FORECASTING DATA

A PREPRINT

 **Stephan Vogt**

Intelligent Embedded System Lab
Kassel University, Germany
Email: stephan.vogt@uni-kassel.de

 **Jens Schreiber**

Intelligent Embedded System Lab
Kassel University, Germany
Email: j.schreiber@uni-kassel.de

 **Bernhard Sick**

Intelligent Embedded System Lab
Kassel University, Germany
Email: b.sick@uni-kassel.de

April 4, 2022

ABSTRACT

Photovoltaic and wind power forecasts in power systems with a high share of renewable energy are essential in several applications. These include stable grid operation, profitable power trading, and forward-looking system planning. However, there is a lack of publicly available datasets for research on machine learning-based prediction methods. This paper provides an openly accessible time series dataset with realistic synthetic power data. Other publicly and non-publicly available datasets often lack precise geographic coordinates, timestamps, or static power plant information, e.g., to protect business secrets. On the opposite, this dataset provides synthetic time-series measurements, input features, geographic information, timestamps, and physical properties of a set of individual power plants. The dataset comprises 120 photovoltaic and 273 wind power plants with distinct sides all over Germany from 500 days in hourly resolution. This large number of available sides allows forecasting experiments to include spatial correlations and run experiments in transfer and multi-task learning. Furthermore, the dataset includes side-specific, power source-dependent, non-synthetic input features from the Icosahedral Nonhydrostatic-European Union. However, since timestamps and location are known, combining the synthetic power measurements with other weather models is also possible. A simulation of virtual power plants with physical models and actual weather measurements provides synthetic power measurement time series. These time series correspond to the power output of virtual power plants at the location of the respective weather measurements. Since the synthetic time series are based exclusively on weather measurements, possible errors in the weather forecast are comparable to those in actual power data. In addition to the data description, we evaluate the quality of weather-prediction-based power forecasts by comparing simplified physical models and a machine learning model. This experiment shows that forecast errors on the synthetic power data are comparable to real-world historical power measurements. The machine learning model consists of gradient boosted regression trees, which show a lower forecast error for wind and photovoltaic with sufficient training data. In addition, we consider truncated datasets and find that, at least for photovoltaics, there is an advantage of the physical approaches when we only use a fraction of the training data. The errors serve as a baseline for future experiments.

Keywords Wind Power / Photovoltaic Forecasting · Synthetic Dataset · Machine Learning

1 Introduction

Renewable energies are taking on an increasing role in modern energy supply systems. As their share increases, the energy supply system’s volatility and dependence on the weather grow. Therefore, energy forecasts are an essential tool to assure grid stability and reduce uncertainty, e. g., in energy markets or planning assets of electrical grids. For this reason, the importance of research on forecasts of wind energy and photovoltaic (PV) systems has increased.

In renewable energy forecasts, we typically utilize weather forecasts, such as the wind speed or radiation, from a so called numerical weather prediction (NWP) model. These predicted weather features are the input to machine learning (ML) models, predicting the expected power generation, e. g., in *day-ahead* forecasts between 24 and 48h into the future. Datasets must be open for researchers from different fields to develop new forecasting techniques that reduce forecast error and decrease uncertainty in the energy system. Open datasets allow to compare newly developed methods, reproduce these results, and compare results to state of the art.

However, the existing datasets usually have various limitations. In some cases, the number of sites considered is relatively small (e.g., in [1]), so it is impossible to make statements with statistical significance. In some cases, the data is anonymized without an exact geographic location and not synchronized in time, see [2] and [3]. Such anonymizations prohibit a model from taking spatiotemporal dependencies into account that are common in the electrical grid. Further static information, e.g., technical conditions such as the orientation of PV modules or the rotor-generator ratio of wind turbines, is often missing. At the same time, when a park has insufficient data for traditional ML techniques, the utilized physical models require this static information. Additionally, these static information are also essential for, e.g., transfer learning (TL) and zero-shot learning techniques [4] that are ML methods to handle limited data. In the future, more and more forecasting techniques only require limited data and provide high-quality forecasts to compensate for the severe increase in volatile energy resources. Additionally, in practical application, i.e., in typical systems of forecast vendors, one has to deal with missing technical information. On the other hand, in research, it is critical to have a dataset as complete as possible and thus to be able to analyze how the lack of such information potentially affects the forecast quality. Therefore, we provide a complete and open¹ accessible dataset that allows researchers to answer various questions in the field of wind and photovoltaic forecasting with ML techniques.

In particular, we provide a large dataset that comprises synthetic but realistic 120 photovoltaic and 273 wind virtual power plant sides for roughly 500 days that includes the most relevant static data. This dataset is the largest open accessible dataset for renewable power forecasts to the best of our knowledge. We assure that the synthetic power measurements are realistic by utilizing meteorological weather measurements and physical models. This consideration is essential as most of the forecast error in energy forecasting relates to the forecast error caused by the input features from the NWP model. The period under consideration starts December 8, 2018, and ends June 2, 2020 with hourly time resolution. The length of 500 days allows a model training to include all seasons in the training set (a year comprises about 75%) and still have sufficient test data (about 25%).

The remainder of this article is structured as follows. First, in Sec. 2, we overview the data and the intended use. We also argue why there is a necessity for such a dataset, e.g., in the context of TL. Afterward, we outline the most relevant types of data utilized for the generation of the dataset in Sec. 3. Based on those definitions, we detail the approaches to generate synthetic power measurements in Sec. 4. Sec. 5 shows our results for power forecasting techniques on the dataset as a baseline for future research. Finally, we summarize our work and suggest future work in Sec. 6.

2 Data Overview and Intended Use

The data per location is divided into input data (`data_input_<location id>.csv`) and target data (`data_target_<location id>.csv`). Both CSV files, input, and target have a timestamp that allows a unique assignment to each other. This timestamp is the prediction time, i.e., the time the prediction is valid. The simplest option is to treat the data as i.i.d. samples (even though they are not). This assumption makes it possible to treat the problem as a non-linear but time-independent regression problem, and many standard supervised ML methods can be applied. Here, the input CSV represents a design matrix (input data matrix) whose individual rows correspond to the rows of the target CSV and the columns correspond to suitable input features. One might not use the raw timestamp as an input feature. Otherwise, the model possibly never generalizes beyond the training period (i.e., the test period, for example). The target-CSV includes a column ‘pw’, which contains the synthetic power measurement and thus the intended target. We generate these targets through a physical model based on *real-world* on-site meteorological weather measurements. As most of the forecast errors in energy forecasts relate to the NWP forecasts, by utilizing real-world meteorological weather measurements, we are capable of providing realistic synthetic power measurements.

¹Currently, the dataset is not accessible through a central data-repository. Therefore, please write us an e-mail in case you require the data.

Furthermore, we provide a test flag and the output of a physical baseline model. To communicate a forecasting model’s final test errors, we recommend the data samples with the test flag. We utilize the same physical model and parametrization that generated the synthetic power for the baseline. However, these forecast Icosahedral Nonhydrostatic-European Union (ICON-EU) NWP forecasts instead of the real-world weather measurements.

Beginning December 1, 2019, a flag marks the beginning of a predefined test period. The test flag should help to better compare results across research groups. We suggest using samples between December 8, 2018, and December 1, 2019, for training and validation (model selection). The test data from a period after December 1, 2019, enables the test of a hypothesis under consideration as independently as possible of the training period. However, it is noteworthy that since the test data were published together with the training data, indirect overfitting may occur unintentionally, for example, if the test dataset is taken into account in some way in the model selection. Therefore, methods compared in this way might not work with a similar advantage on future, previously unknown data. Nevertheless, it can help to assess the capabilities of investigated methods better.

2.1 Forecasting Scenarios

We created the dataset with a day-ahead forecasting scenario in mind, which is typical for many forecasting vendors. At the same time, day-ahead forecasts are more challenging than intra-day forecasts, as with an increasing forecast horizon of the weather model, the error of the input features increases. Based on current literature [5] and exchanges with experts from the industries, we identified the following key research areas:

- **Single task forecasting** is still ongoing research and recent developments from the field of deep learning allow to reduce the forecast error and thereby decrease the uncertainty for the electrical grid.
- Regional estimation of wind / PV power production, which take **geospatial dependencies** into account, better capture the dynamics in the electrical grid.
- **Multi-task learning** reduces the forecast error, the number of parameters, and the training time [6, 7]. Effectively, this technique helps in compensating for the high demand for forecasts.
- **Transfer learning** allows for reducing the training time and the required number of historical power measurements that are often not available [7, 4].
- **Meta-learning** and similarly **zero-shot learning** ideally allow to provide power forecasts without any historical data [4] and are, e.g., an essential technique to provide forecasts for new power plants without any historical data.
- **Explainable ML** allows participants in the energy systems to make justified decisions.

3 Data Basis

Three different data sources play a role in synthesizing power forecasting data, namely meteorological measurements, numerical weather predictions, and static (metadata) data for the individual power plants. The static data forms the parametrization of the physical models. Furthermore, this model simulates the power output based on meteorological measurements. Besides, the numerical weather predictions provide the necessary input features, which currently form our best source for information about future weather conditions in a short-term range (within a few days).

3.1 Meteorological Measurements

Since photovoltaic and wind energy depends highly on the local weather conditions, meteorological data form the basis for the synthetic data. The power output of a single plant forms the target variable in many photovoltaic and wind power forecasting tasks. Typically, power plants have a quick response to changes in weather conditions, and therefore the variability of the relevant weather variables is almost directly transferred to the power output. Meteorological measurements, such as wind speed or global horizontal irradiation, can provide a realistic degree of variability and randomness as the basis for the target data.

In addition, meteorological measurements accurately represent spatial and temporal relationships of the underlying atmospheric state in equal measure. Figure 1 shows the spatial distribution of the measurement sites. At the same time, these sites represent the virtual locations of the power plants, i.e., wind energy or photovoltaic power plants, which correspond to the synthetic data. The plot shows that wind speed measurements are also available at all locations where radiation data is available. The reverse is not applicable, so less than half of the sites have radiation measurements. The underlying measurements for solar are from [8] and the wind resource measurements from [9].

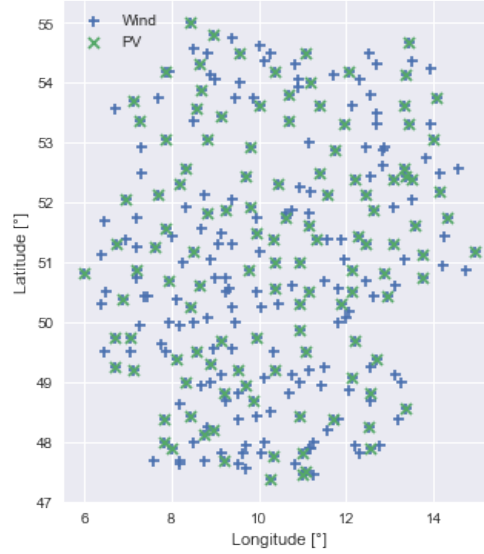


Figure 1: Geographical locations of weather measurements, respective sides of the synthetic power measurements.

3.2 Input Features and Numerical Weather Prediction

We take input features from the ICON-EU weather model as a basis, described in [10]. These numerical weather predictions were computed and provided by the German Meteorological Service (*Deutscher Wetterdienst*) and provided for this study by Fraunhofer IEE. For PV- and wind energy, several features were extracted and processed individually. In contrast to the surface synoptic observation (SYNOP) measurements, the features from the ICON-EU model are available within the considered forecast horizons (day-ahead scenario) with hourly resolution. The hourly resolution available here forms the basis for the final merged dataset.

Photovoltaic Input Feature

The features for the PV forecast are listed below, with feature names based on those in [10]:

fcst_time Forecast date and time for which the forecast is to be generated and to which the below-mentioned features refer to in the format `yyyy-mm-dd HH:MM:SS [UTC]`.

nwp_fcst_horiz_hours forecast horizon in relation to the start of the numerical weather prediction model run at 00:00 of the previous day [h].

T_HAG_2_M Air temperature 2m above the earth's surface [$^{\circ}\text{K}$].

RELHUM_HAG_2_M Relative humidity 2m above earth surface [%].

PS_SFC_0_M Air pressure at the earth's surface [Pa].

U_GVL_60_HL Zonal wind speed (wind parallel to latitude) at about 10m above ground [m/s].

V_GVL_60_HL Meridional wind speed (longitude-parallel wind) at about 10m above ground [m/s].

ASWDIFDS_SFC_0_M_INSTANT Instantaneous solar diffuse radiation at the earth's surface with a time lag relative to the forecast time of -1h, 0h, or +1h (three features with the suffixes `_m1_`, `_`, or `_p1`) [W/m^2].

ASWDIRS_SFC_0_M_INSTANT Instantaneous solar direct radiation at the earth's surface with a time lag related to the prediction time by -1h, 0h or +1h (three features with suffixes `_m1_` or `_p1`) [W/m^2].

solar_azimuth Azimuth angle of the sun position calculated using prediction time and the toolbox PVLib, described in [11] [$^{\circ}$].

solar_zenith Zenith angle of the sun position calculated using prediction time and Toolbox PVLib.

Except for the prediction time `fcst_time`, these features can be used directly as inputs for nonlinear regression models. We use `fcst_time` to assign the time to the corresponding target value, to other weather models, or to calculate additional features, e.g., representing the season. Nevertheless, `fcst_time` is less suitable as a direct input feature in

the case of ML methods since the test data will differ in the considered time and therefore, an ML model will most likely not generalize well.

Irradiance features ending with `_INSTANT` differ from the original weather model quantities due to our post-processing of original irradiance values. In the ICON-EU weather model, these quantities are stored as mean values since the beginning of the model run. Since we aim to predict the instantaneous power of the system, we convert these quantities to instantaneous irradiance features through the differences between temporally adjacent time steps.

In total, the synthetic PV dataset thus contains 15 different features, 14 of which can be used directly as input to a regression model.

Wind Power Input Feature

In the case of the synthetic wind power data, the data are available with 19 comparable input features, which we describe in detail in the following list:

fcst_time Forecast date and time for which the forecast is to be generated and to which the below-mentioned features refer to in the format `yyyy-mm-dd HH:MM:SS [UTC]`.

nwp_fcst_horiz_hours is the forecast horizon in relation to the start of the numerical weather prediction model run at 00:00 of the previous day [h].

T_HAG_2_M Air temperature 2m above the earth's surface [$^{\circ}\text{K}$].

RELHUM_HAG_2_M Relative humidity 2m above earth surface [%].

PS_SFC_0_M Air pressure at the earth's surface [Pa].

U_GVL_58_HL Zonal wind speed (wind parallel to latitude) at about 100m above ground with a time lag related to the forecast time of -1h, 0h or +1h (three features with suffixes `_m1,_` or `_p1`) [m/s].

V_GVL_58_HL Meridional wind speed (longitude-parallel wind) at about 100m above ground with a time lag related to the forecast time of -1h, 0h or +1h (three features with suffixes `_m1,_` or `_p1`) [m/s].

U_GVL_60_HL Zonal wind speed (wind parallel to latitude) at about 10m above ground with a time lag related to the forecast time of -1h, 0h or +1h (three features with suffixes `_m1,_` or `_p1`) [m/s].

V_GVL_60_HL Meridional wind speed (longitude-parallel wind) at about 10m above ground with a time lag related to the forecast time of -1h, 0h or +1h (three features with suffixes `_m1,_` or `_p1`) [m/s].

ASWDIFDS_SFC_0_M_INSTANT Instantaneous solar diffuse radiation at the Earth's surface [W/m^2].

ASWDIRS_SFC_0_M_INSTANT Instantaneous solar direct radiation at the Earth's surface [W/m^2].

3.3 Static Data

We summarize the static data (or metadata) for all locations of the respective energy source in the file `meta.csv`. The individual rows in the CSV represent the static data for the individual locations. For both wind and PV, the file contains the identification number (`loc_id`), the geographical coordinates (`longitude` or `long` and `latitude` or `lat`), the file names of the associated input and target data (`input_file_name` and `target_file_name`), and a brief statistic in form of the number of samples per sample set (`num_train_samples`, `num_test_samples`). Further static data differ depending on the energy source, especially the physical parametrization.

Photovoltaic Parametrization

In the case of photovoltaics, one finds information about the module, the inverter, and the wiring (modules per string and strings per inverter). However, we selected only one configuration for simplicity, namely module: Canadian Solar CS5P 220M (2009), inverter: ABB Micro 0 25 I OUTD US 208 (208V), with one single module per string, and one string per inverter. We chose this configuration based on the experience that the exact module and inverter parameters (e.g., rated power, efficiency, and temperature coefficients) have a relatively small impact on the prediction quality, especially after normalization and compared to the errors of the weather model. Much more important, however, is the exact orientation of the plant. The orientation parameters are drawn from a random distribution to have a diverse collection of different orientations in the dataset. We sample the module tilt angle from a uniform distribution in the interval between 0° (flat) and 90° (vertical). Similarly, we sample the azimuth angle from a uniform distribution between 90° (east) and 270° (west), with the south defined as 180° .

Wind Power Parametrization

We summarize similar information about the simulated wind turbines in the corresponding `meta.csv` file associated with the synthetic wind power dataset. The file includes the hub height used for vertical interpolation, the rotor diameter in meters, and the nominal power in kilowatts. Additionally, we provide information about the respective turbine type. The latter information is crucial to be able to reproduce the dataset since the corresponding power curves were stored as manufacturer information in the simulation, similar to [12]. The turbine power curve and the hub height of each entry in `meta.csv` were individually selected by randomly choosing one of the possible hub heights (either maximum or minimum) and one specific turbine type.

4 Synthetic Data Generation

This section describes in detail how we assemble the datasets. Fig. 2 depicts the overall concept. On the left, various data sources are listed. We process those data sources either through a physical model or feature pre-processing. The resulting output of the synthetic data generation, namely target and input data, is given on the right.

The top row, the top grey box, shows the process to synthesize the target data. In this process, a power model transforms meteorological measurements (SYNOP) and static plant configurations into a power time series. The used power models are implemented either as a physical model (PV) or are given as an empirical look-up table by the power plant manufacturers (power curves of wind turbines). The resulting time series represents the synthetic power measurement, which we provide as a target for a ML-based forecasting model. Note that we do not use numerical weather prediction data to prepare the target data. This process ensures that the expected forecast errors are similar in magnitude and characteristics to real-world power forecasts.

The bottom row, the bottom grey box, shows the process of input data preparation. The raw input features include numerical weather predictions and the corresponding time stamp information at the nearest weather model grid node to the measurements side. Depending on the energy source, certain features are selected and pre-processed. This feature processing consists, for example, of the time-lags of specific input signals concerning the prediction time. The motivation for this is to provide samples that can even be used in regression models that make an i.i.d. assumption. Other features, such as sun angles in the case of photovoltaics, are also calculated and provided.

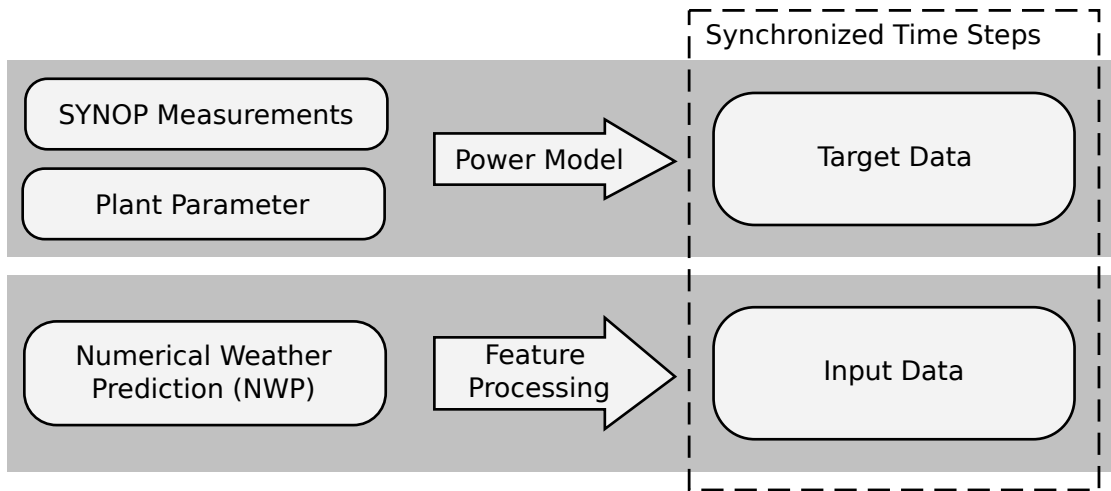


Figure 2: Flowchart for synthesizing power data from weather measurements and of the feature extraction process.

Furthermore, on the right side, there is a dashed box. This box symbolizes the synchronization of the input data and the target variable. This synchronization takes place according to a day-ahead forecast. Here, a scenario was set, which assumes the daily creation of a day-ahead forecast. More precisely, we assume that the 00:00 o'clock model run of the weather model is delivered to the power forecast provider. Related to the origin of the 00:00 model run, we synchronize the forecast horizons between 24h and 47h inclusive with the power values with hourly resolution. The hourly resolution of the weather prediction is adopted by down-sampling the weather measurements, which initially have a 10min time resolution. Therefore, interpolation is not needed. Furthermore, for each geographic power plant location, the predictions of the nearest point of the NWP grid were extracted.

4.1 Photovoltaic Power Model

Radiance measurements are converted via a physical model into power measurements to generate the synthetic power measurements. The underlying physical model is the one from the simulation toolbox PVLlib [11]. All simulations use the same photovoltaic module type *Canadian Solar CS5P-220M (220W) Solar Panel* which is specified in more detail in [13]. Similarly, the same type of inverter was used exclusively for all simulations, namely the *MICRO-0.25/0.3/0.3HV-I-OUTD-US-208/240* described in [14]. We assume that all PV power plants contain only a single module as an additional simplification. The synthetic measurement time series are normalized by the installed capacity, i.e., the module peak power.

The SYNOP-power measurements include the ten-minute sum of incoming solar radiation in Joule per cubic Centimeter and the ten-minute sum of the diffuse solar radiation with the same unit. PVLlib expects the global horizontal irradiance (GHI), the direct normal irradiance (DNI) and the diffuse horizontal irradiance (DHI) in Watt per square Meter, as well as wind speed and air temperature. To overcome this difference, we transformed the measured quantities accordingly by using the methods given in PVLlib, i.e., *pvl-lib.irradiance.dni* to estimate DNI based on GHI, DHI and Zenith angle. Previously, the zenith angle was computed based on the geographic position and time, while GHI and DHI are transformed under the assumption of a discrete approximation of the energy-time derivative, i.e., that the power is the ratio of a discrete change in energy in a given time interval. Wind speed and air temperature remained with their PVLlib-default values of 0m/s and 20° Celsius for further simplification.

Finally, the simulation requires information about the location. This information includes the geographic coordinates, which correspond to the coordinates of the weather measurement and the altitude. For simplicity, we assume the altitude to be 0m above sea level. All other model inputs, such as the albedo, were left at the PVLlib default values.

Figure 3a and Figure 4 show the simulated PV power in relation to the predicted direct irradiation on a horizontal plane. An increase in irradiation leads to an expected increase in the power generation in figure 3a. At the same time, the inherent uncertainty of the weather prediction and the missing consideration of the module orientation leads to a spread of the point cloud in the y-direction. This difference is also a typical behavior in real-world datasets.

Figure 4 shows the normalized power output (blue line) of the same plant in a three-week window together with the normalized horizontal direct irradiation (yellow line). The slight shift of the blue curve, compared to the yellow curve, to the right results from a slight west-ward orientation of the simulated PV module. While sunny days predominantly show agreement in the yellow and blue curve profile, cloudy days show more extensive and random deviations between the synthetic power data and the predicted solar resource. That is typical and results from the NWP difficulties to predict exact cloud positions. Furthermore, the predicted solar resources appear to fluctuate less than the synthetic power generation. This difference in fluctuation also results from the properties of the NWP, which rather forecasts an expected value of a local patch (several thousand meters in size) compared to the local point of the single plant and, with that, to smooth out any detailed cloud structures.

4.2 Wind Energy Power Model

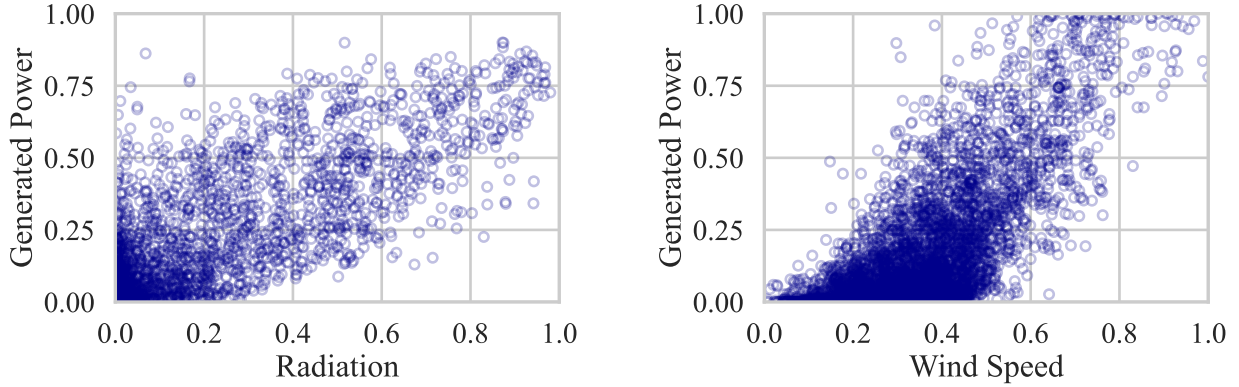
A simple power curve model was used to calculate wind power. In the first step, we extrapolate the measured wind speed u_{ref} from 10m height to the height of the turbine. For this purpose, the so-called wind profile power law is applied, described in [15]. With that, we compute the wind speed at the height of the wind turbine u_{ref} with

$$u = u_{ref} \left(\frac{z}{z_{ref}} \right)^\alpha, \quad (1)$$

where the hub height z of the wind turbine, the measurement height $z_{ref} = 10m$, the measured wind speed u_{ref} and a stratification coefficient $\alpha = \frac{1}{7}$ (assumption of neutral stratification) are used. In the next step, a linear interpolation is applied together with a lookup table of the manufacturer's power curve as given in [12]. Each power curve lookup table is defined in terms of reference wind speeds and reference power measurements, discretized with a resolution of 1 m/s up to a maximum reference wind speed of 25 m/s. Other possible impact factors, such as air density, turbulence, or atmospheric stability are ignored for simplicity.

Figure 5 shows the temporal development of the generated wind power output, normalized by the plant capacity, of a single wind power plant for a three-week window as an example. Due to the characteristic properties of the power curve, there is no feed-in power at very low wind speeds (ca. < 1-2 m/s). If high wind speeds occur (ca. > 12 m/s), the generation is limited by the nominal power of the wind turbine. These properties form the characteristic shape of such wind power time series.

At the same time, the yellow curve shows the forecasted wind speed. Here we can observe that wind speed and power are correlated since higher predicted wind speeds also tend to have higher power values. This correlation becomes even more evident in figure 3b, where the generated power, the synthetic measurement, is plotted above the predicted wind speed, given by the NWP. The typical S-shaped course of the power curve appears here. At the same time, however,



(a) Feed-in of a virtual PV plant plotted against direct-horizontal radiation (ICON-EU).

(b) The output of a virtual wind turbine over the magnitude of the predicted wind speed vector (ICON-EU).

Figure 3: Scatter plots of the synthetic power generation (SYNOP based) over the corresponding predicted weather resource.

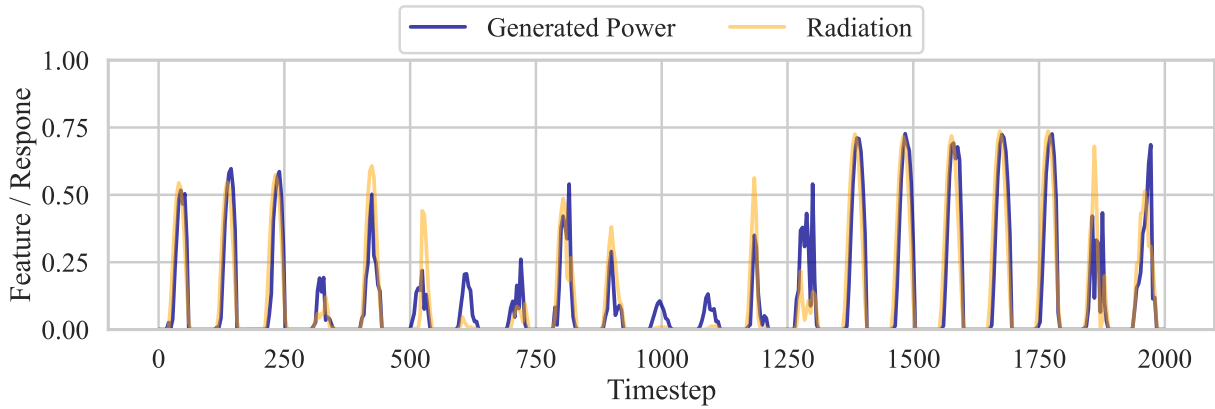


Figure 4: Exemplary three weekly course of the synthetic power generation of a virtual PV power plant and the irradiation normalized with the nominal power and 1000 W/m^2 . The data was linearly interpolated to a 15-minute resolution.

there is also a wide spread. The spread, as in the case of PV, is due to the forecast errors of the weather resource. Analogously to PV, this uncertainty is close to the real world and thus also shows up in actual wind power forecast data.

5 Experimental Results

The following section conducts an experiment that serves as the baseline for future research. Moreover, the experiment allows comparing forecast errors of the proposed synthetic dataset with real-world forecast errors, showing our dataset’s applicability for future research in renewable power forecasts. We evaluate physical forecasting techniques on the introduced datasets within the following experiment. Physical approaches are essential as they are typically utilized when only limited data is available for training. At the same time, there is an increasing interest in providing high-quality forecasts through ML models even with limited data. Therefore, we compare the results of physical models with the gradient boosting regression tree (GBRT). We choose the GBRT here as it generalizes well with a limited amount of data and is known to mitigate the effects of overfitting.

To assess the forecast quality of the GBRT concerning reduced data, as it is common with TL, we limit the training data to the last 7,14,30,60 or 90 days of training data of a season. Respectively, we repeat this experiment for each season’s different number of training data to ensure that results account for seasonal patterns. To increase the number of training data within this scenario, we linearly interpolate the data to have a 15-minute resolution. Additionally, we make one experiment where we consider the complete training data, indicated through 365, and compare those forecast errors

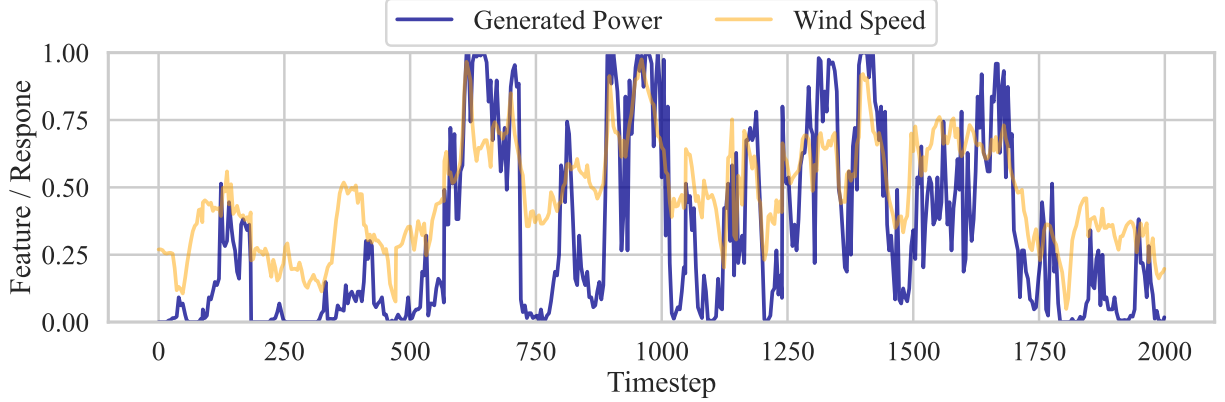


Figure 5: Three-week history of synthetic power generation from a virtual wind turbine and the predicted underlying wind speed normalized by the rated power and maximum wind speed, respectively. The data was linearly interpolated to a 15-minute resolution.

with an example from real-world datasets. We consider time steps with the test flag as test data and the remaining data as training data.

Most often the forecast error, in renewable power forecast, is determined by the normalized root mean squared error (nRMSE) given by

$$\text{nRMSE} = \sqrt{\frac{1}{N} \sum_{i=0}^{i=N} (y_i - \hat{y}_i)^2}, \quad (2)$$

where y_i is the i -th normalized response from the target and \hat{y}_i is the prediction from a source model on the target. Note that in the context of renewable power forecasts, we normalize the response y_i by the nominal power to assure comparability of the error for different parks. To express an improvement of one model over another model we utilize the skill given by

$$\text{Skill} = \text{nRMSE}_{\text{gbrt}} - \text{nRMSE}_{\text{phy}}, \quad (3)$$

where $\text{nRMSE}_{\text{gbrt}}$ is the nRMSE of the GBRT model and $\text{nRMSE}_{\text{phy}}$ of the physical model, respectively. Consequently, values below zero indicate an improvement of the GBRT over a physical forecasting technique.

We optimize the GBRT for each park, season, and number of training data through a grid search by three-fold cross-validation based on the available training data. Thereby, the learning rate is evaluated at $[10^{-6}, 3.1 \times 10^{-6}, \dots, 3.1 \times 10^{-1}, 1]$. The number of estimators is 300 and the maximum depth is one of $[2, 4, 6, 8]$. Other values are the default ones of scikit-learn ².

We utilize the same parametrization for the physical models for creating the power measurements. The only difference is that we now use the direct radiation and wind speed, respectively, from the NWP as input. The physical model for the wind dataset is indicated through *Enercon* in the following and *PV Physical* for the PV dataset. Additionally, for the wind dataset, we compare the GBRT results with empirical *McLean* power curves [16]. This power curve is well known and considers typical influences by different terrains.

PV day-ahead power forecasting problems often have an nRMSE between 0.06 and 0.12 [17]. The mean nRMSE values of the PV baseline is at 0.085 on the proposed synthetic dataset, see Tbl. 1. Forecast errors of the GBRT model are between 0.12 and 0.072 depending on the amount of available training data. With an increasing amount of training data, the forecast error reduces for this model. The mean forecast error of the GBRT is only better with the complete training data. Fig. 6 shows the evaluation concerning the skill for the PV dataset. Up to 14 days of training data, the GBRT model has substantial positive outliers of the skill. With additional training data, this effect reduces. Beginning from 60 days of training data, the median skill is close to zero, indicating the GBRT is as good as the physical baseline in most cases. With 90 days of training data and the complete dataset, the GBRT has improvements over the physical baseline.

Tbl. 2 summarizes the mean nRMSE for the wind dataset. The Enercon baseline has a mean nRMSE of 0.21. Wind day-ahead power forecasting problems typically have an nRMSE between 0.1 and 0.2 [17]. Depending on the utilized empirical McLean power curve, forecast values of this approach range between 0.212 and 0.228. The GBRT forecasting

²<https://scikit-learn.org/>, Version 0.24, accessed 2022-02-28

Table 1: Mean nRMSE values of the GBRT across all available parks for different amounts of training data in comparison to physical models for the PV dataset. Best values for the amount of training data are highlighted in bold.

Number of Days	GBRT	PV Physical
7	0.120	0.085
14	0.107	0.085
30	0.092	0.085
60	0.089	0.085
90	0.086	0.085
365	0.072	0.085

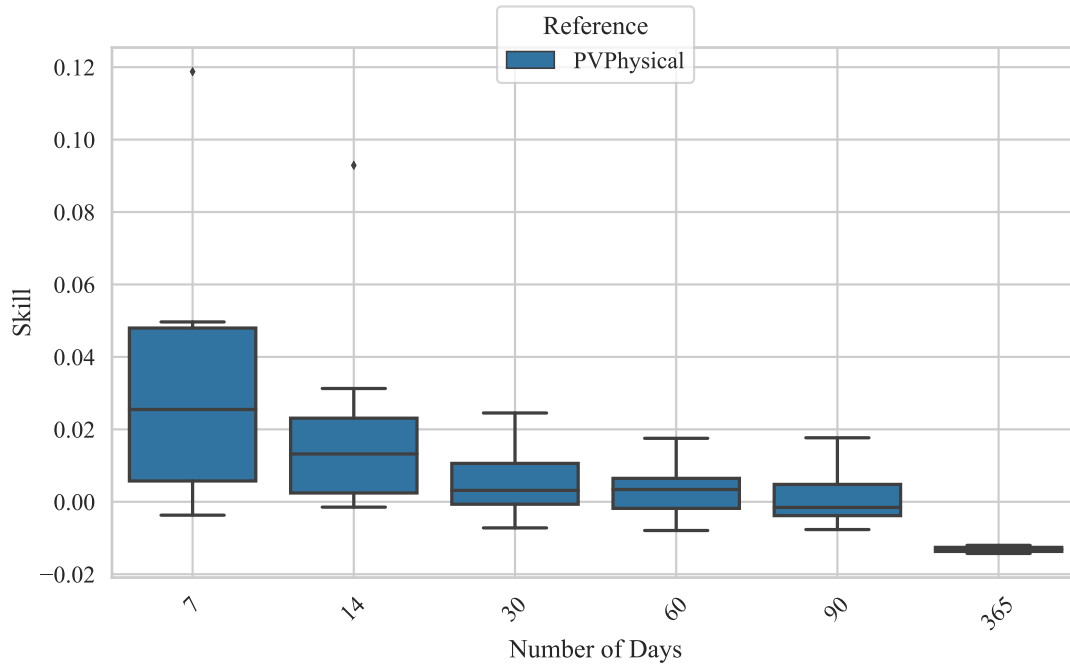


Figure 6: Skill between the GBRT model and the physical baseline of the dataset for the PV dataset. Values below zero indicate an improvement of the GBRT over the physical reference.

technique has the best mean nRMSE for all numbers of available training data. With seven days of training data, the GBRT has an nRMSE of 0.196, with 90 days of training data a nRMSE of 0.147, and with the complete data, an error of 0.125. The improvements of the GBRT over the other models are also given through the skill in Fig. 7. In contrast to results from the PV dataset, the median skill is below zero already with seven days of training data. However, with less than 30 days of training data, substantial outliers are present compared to the Enercon baseline. These are not present with more than 30 days of training data.

All in all, we can observe that the forecast error of the physical baseline and, in particular, errors from the ML technique are comparable to those given by real-world power measurements. For the PV dataset, we see that the physical baseline is robust, especially in the case of limited data. At the same time, these excellent results also relate to the fact that the exact physical characteristics are given, which is most often not the case in real-world forecasting problems. In the case of the proposed wind dataset, the GBRT provides a strong baseline for future research. In a comparison of those two datasets, the physical approach for the PV dataset considers more physical characteristics in comparison to the Enercon baseline. At the same time, the PV power forecasting problem can be considered more linear in contrast to wind power forecasts, which makes it easier to model all dependencies within a physical baseline. Interestingly, errors of the *McLean-Upland* empirical power curve are close to that of the Enercon baseline. This observation lets us conclude that it is a suitable baseline for limited data when a wind turbine’s physical characteristics are not given.

Table 2: Mean nRMSE values of the GBRT across all available parks for different amounts of training data in comparison to the physical model and different McLean power curves for the wind dataset. Best values for the amount of training data are highlighted in bold.

	GBRT	Enercon	McLean-Lowland	McLean-Lowland-Regulated	McLean-Offshore	McLean-Upland
Number of Days						
7	0.196	0.210	0.228	0.216	0.239	0.212
14	0.178	0.210	0.228	0.216	0.239	0.212
30	0.156	0.210	0.228	0.216	0.239	0.212
60	0.154	0.210	0.228	0.216	0.239	0.212
90	0.147	0.210	0.228	0.216	0.239	0.212
365	0.125	0.210	0.228	0.216	0.239	0.212

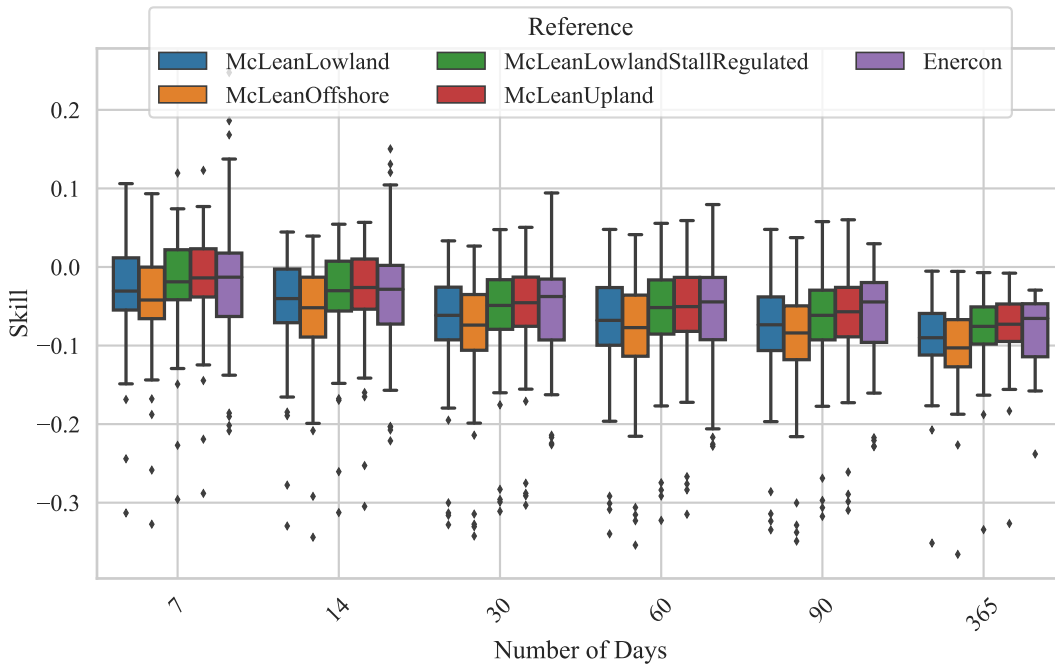


Figure 7: Skill between the GBRT model and the physical baseline (Enercon) and different McLean power curves for the wind dataset. Values below zero indicate an improvement of the GBRT over those references.

6 Conclusion and Future Work

We successfully created a realistic wind and photovoltaic power forecast dataset within the article. Power measurements are generated based on real-world weather measurements, ideal for creating power time series through physical models. At the same time, considering numerical weather prediction as input features for the ML model, results show that forecast errors are in line with other real-world renewable power datasets. By providing metadata for each plant, we provide the possibility for transfer learning, multi-task learning, and zero-shot learning for future research by considering those physical characteristics.

Acknowledgments This work has been partially carried out within the project TRANSFER (01IS20020B) funded by BMBF (German Federal Ministry of Education and Research) and the research project gridcast (Fkz. 0350004A) funded by the BMBK (German Federal Ministry for Economic Affairs and Climate Action). Furthermore, we would like to express our special thanks to the German Weather Service (DWD) and the Fraunhofer Institute for Energy Economics and Energy System Technology (IEE) for providing the weather data.

References

- [1] Tao Hong, Pierre Pinson, and Shu Fan. Global energy forecasting competition 2012, 2014.
- [2] Andre Gensler, Janosch Henze, Bernhard Sick, and Nils Raabe. Deep Learning for solar power forecasting — An approach using AutoEncoder and LSTM Neural Networks. In *IEEE International Conference on Systems, Man, and Cybernetics (SMC)*, pages 002858–002865. IEEE, 2016.
- [3] André Gensler, Bernhard Sick, and Vitali Pankraz. An analog ensemble-based similarity search technique for solar power forecasting. In *2016 IEEE International Conference on Systems, Man, and Cybernetics (SMC)*, pages 002850–002857, 2016.
- [4] Jens Schreiber, Stephan Vogt, and Bernhard Sick. Task Embedding Temporal Convolution Networks for Transfer Learning Problems in Renewable Power Time-Series Forecast. In *ECML*, 2021.
- [5] Ghadah Alkhayat and Rashid Mehmood. A review and taxonomy of wind and solar energy forecasting methods based on deep learning. *Energy and AI*, 4:100060, 2021.
- [6] Jens Schreiber and Bernhard Sick. Emerging Relation Network and Task Embedding for Multi-Task Regression Problems. In *International Conference on Pattern Recognition*, 2020.
- [7] Stephan Vogt, Axel Braun, Jan Dobschinski, and Bernhard Sick. Wind Power Forecasting Based on Deep Neural Networks and Transfer Learning. In *18th Wind Integration Workshop*, page 8, 2019.
- [8] Dwd climate data center (cdc): Historical 10-minute station observations of solar incoming radiation, longwave downward radiation and sunshine duration for germany, version v1. https://opendata.dwd.de/climate_environment/CDC/observations_germany/climate/10_minutes/solar/. Accessed: 2020-09-06.
- [9] Dwd climate data center (cdc): Historical 10-minute station observations of mean wind speed and wind direction for germany, version v1. https://opendata.dwd.de/climate_environment/CDC/observations_germany/climate/10_minutes/wind/historical/. Accessed: 2020-09-06.
- [10] Daniel Reinert, Helmut Frank, and Florian Prill. *ICON database reference manual*. Deutscher Wetterdienst, 2016.
- [11] William F. Holmgren, Clifford W. Hansen, and Mark A. Mikofski. pvlib python: a python package for modeling solar energy systems. *Journal of Open Source Software*, 3(29):884, 2018.
- [12] Enercon GmbH. *ENERCON Produktübersicht*, 6 2015.
- [13] SolarDesignTool. *Canadian Solar CS5P-220M*, accessed January, 2022.
- [14] fimer.com. *Product manual MICRO-0.25/0.3/0.3HV-I-OUTD-US-208/240*, 2014 (accessed January, 2022).
- [15] Jawad S Touma. Dependence of the wind profile power law on stability for various locations. *Journal of the Air Pollution Control Association*, 27(9):863–866, 1977.
- [16] F. Van Hulle, J. O. Tande, K. Uhlen, et al. Further Developing Europe’s Power Market for Large Scale Integration of Wind Power - Equivalent Wind Power Curves. *European Wind Energy Association (EWEA)*, 2008.
- [17] Jens Schreiber, Malte Siefert, Kevin Winter, Arne Wessel, Rafael Fritz, Garrett Good, André Schella, Jewgenija Muraschko, and Stefan Staedler. Abschlussbericht Projekt Prophecy : Prognoseunsicherheiten von Windenergie und Photovoltaik in zukünftigen Stromversorgungssysteme. *German National Library of Science and Technology*, page 168, 2020.